Magnonic spectral gaps and discrete transmission in serial loop structures

2002 J. Phys.: Condens. Matter 14 637

(http://iopscience.iop.org/0953-8984/14/3/331)

INSTITUTE OF PHYSICS PUBLISHING JOURNAL OF PHYSICS: CONDENSED MATTER

J. Phys.: Condens. Matter **14** (2002) 637–655 PII: S0953-8984(02)28188-6

Magnonic spectral gaps and discrete transmission in serial loop structures

A Mir[1], H Al Wahsh[2], A Akjouj[3], B Djafari-Rouhani, L Dobrzynski and J O Vasseur

Laboratoire de Dynamique et Structures des Matériaux Moléculaires, ESA CNRS 8024, UFR de Physique, Université de Lille1, 59655 Villeneuve d'Ascq Cédex, France

E-mail: Abdellatif.Akjouj@univ-lille1.fr

Received 23 August 2001
Published 8 January 2002
Online at stacks.iop.org/JPhysCM/14/637

Abstract

In the frame of the long-wavelength Heisenberg model, the magnonic bandgaps and the selective transmission in a serial loop structure, made of loops pasted together with segments of finite length, are investigated theoretically. The loops and the segments are assumed to be one-dimensional ferromagnetic materials. Using a Green function method, we obtained closed-form expressions for the band structure and the transmission coefficients for an arbitrary value of the number N of loops in the serial loop structure. It was found that the gaps originated from the periodicity of the system. The width of these forbidden bands depends on the structural and compositional parameters. We also present analytical and numerical results for the transmission coefficient through a defective geometry where the length of one finite branch has been modified. It was demonstrated that the presence of this defect in the structure can give rise to localized states inside the gaps. We show especially that these localized states are very sensitive to the size of the loops and to the periodicity as well as to the length and the location of the defect branch.

1. Introduction

In recent years low-dimensional spin systems—i.e. magnetic structures with a dimensionality smaller than three—have brought both theoretical and experimental interest [1–3]. The remarkable progress achieved during the past decade in lithographic techniques now allows the fabrication of high-quality, well controlled laterally defined magnetic structures, for example dots and wires, of micrometre or submicrometre sizes. Although static properties of

[1] Permanent address: Département de Physique, Faculté des Sciences, Université Moulay Ismail, Meknès, Morocco.
[2] Permanent address: Faculty of Engineering, Zagazig University, Benha Branch, Cairo, Egypt.
[3] Author to whom correspondence should be addressed.

0953-8984/02/030637+19$30.00

micrometre-size magnetic dots and wires have been studied to some extent [4–7], their high-frequency dynamic properties have been rarely investigated [8, 9]. The study of spin waves is a powerful method for probing the dynamic properties of magnetic media in general and those of laterally patterned magnetic structures in particular [10]. On the other hand, due to the possible use of electron spin for storage and information transfer in quantum computers [11], there have been many recent studies on spin transport in semiconductor nanostructures [12]. In the last decade, several studies have addressed the problem of spin wave band structures in magnetic superlattices [13–16] and two-dimensional (2D) magnetic periodic structures [17]. Most of these studies focus on the existence of stop bands in the spin wave spectra of magnetic structures. More recently, we proposed [18] a model of one-dimensional magnonic crystals exhibiting very narrow pass bands separated by large forbidden bands, following similar studies in photonic and electronic bandgap materials. This system (called a comb structure) is composed of an infinite one-dimensional waveguide along which an infinite or a finite set of side branches is grafted periodically. The presence of defect branches in the comb structure can give rise to localized states within the gaps. It has been shown that these states are very sensitive to the length and number of the side branches, to the periodicity of the system and to the length of the defect branches.

Interest in the systems exhibiting complete or pseudo-gaps was initiated by the pioneering work of Yablonovitch on the macroscopic photonic crystals in 1987 [19]. These systems are useful from both the practical and the fundamental point of view. From the fundamental point of view, Yablonovitch [19] emphasized the inhibition/prohibition of the spontaneous emission due to the existence of the photonic bandgaps. John had simultaneously stressed that the existence of the complete photonic bandgaps could lead to the Anderson localization of light [20] in slightly disordered photonic crystals [21]. From the practical point of view, such systems can be used to design filters that prohibit waves at certain frequencies while allowing free propagation at others. Since then the subject has stimulated a widespread interest in various analogous systems. We refer to those using, for example, elastic waves [22], acoustic waves [23], spin waves [17] and electron waves [24]. These properties also began to be investigated in quasi-one-dimensional photonic crystals [25–27].

Advances in modern semiconductor technology, which have permitted the fabrication of nanostructures with controllable chemical composition and geometry—such as quantum wires, dots, rings, crossbars etc [28]—suggest the possibility of designing and manufacturing networks of one-dimensional magnetic wires [29]. For example, arrays of very long ferromagnetic nanowires of Ni, permalloy and Co, with diameters in the range of 30–500 nm have been created [30]. These are very uniform in cross section, with lengths in the range of 20 μm. They are thus realizations of nanowires one can reasonably view as infinite in length, to an excellent approximation. Besides the static and magneto-transport properties of magnetic nanowire arrays, the dynamic properties of magnetic nanostructures are also of considerable interest in both fundamental and applied research [31]. These recent developments encouraged us to continue our theoretical investigation of magnetic excitations in networks composed of one-dimensional continuous magnetic media. Our choice of one-dimensional magnetic structures is motivated by possible engineer spin injection devices that render feasible the control of the widths of the pass bands (and hence the stop bands).

A model Hamiltonian which considers the exchange energy, the uniaxial anisotropy and the Zeeman energy would be very convenient to discuss various properties of magnetic periodic structures. However, in the present work, in order to neglect the quantum size effect (or the sub-band structure), we shall deal with a magnetic network where the cross-sections of all wires are considered to be much smaller than the considered wavelength. Therefore a continuum approximation was convenient for us to use. Such an approximation is valid provided that the

relevant wavelengths are large compared with the lattice spacing, i.e. we shall deal only with long-wavelength excitations. Therefore, in using the Heisenberg model of a ferromagnet we are neglecting the dipole–dipole interactions compared with the exchange contribution to the Hamiltonian [18, 32]. This macroscopic approach is analogous to that used by Cottam [33] in magnetostatic calculations. Let us mention also that the continuum theory used here has the advantages that explicit analytic expressions of different magnetic properties (dispersion curves, density of states, transmission coefficients, ...) can be calculated.

The Green function (response theory) method used in the calculation in this paper derives a response function which contains all the physical information on the composite system under study. This response function in particular gives directly the magnetization at any point of the system as a response to an unit input excitation introduced at any other point. This method is equivalent to the usual calculation of the eigenvalues and eigenvectors of the composite system in particular by the transfer matrix method [14,15]. Its advantages are in a more compact treatment of the interface boundary conditions and in the fact that this response function enables direct calculations of all the physical properties, in particular of those connected with defects and scattering problems [32]. These Green functions enable us to obtain analytic expressions for the dispersion relation as well as the reflection and transmission coefficients through the structure. The complete response functions can also be used to derive all eigenvectors [34] in the finite networks.

In this paper, we present results on the magnonic band structures and transmission coefficients for a new geometry of one-dimensional magnonic crystals: the serial loop structures (SLSs) (see figure 1). The geometry of the structures has the peculiar property of giving rise to transmission gaps. These transmission gaps occur at particular frequencies that are related to the length and to the physical characteristics of the constituents. These frequencies broaden into absolute gaps as the loop number N increases. The results reported here demonstrate that the widths of the pass bands (and hence of the stop bands) in the serial loop magnonic band structure can be controlled by modifying appropriately the geometry and the chemical nature of the network's constituents. In addition to the excitation spectra of SLSs, we have also calculated the transmission spectra of finite ones. Finally, we address the issue of the existence of localized states in the forbidden bands of the magnonic band structure. Such localized states result from the presence of a defect segment inside the waveguide. Let us stress that in a comb structure [18] an important difficulty lies in the technical realization of the boundary condition at the free ends of the resonators, while this problem is avoided in SLSs.

This study is organized as follows. In section 2, we deal with infinite and finite SLSs. First we use the semi-classical torque equation for the magnetization and the GFM to write down the magnetic GF for an infinite Heisenberg ferromagnetic medium. We then calculate the dispersion relation for SLSs and the transmission coefficients with and without defects. In section 3, we illustrate these analytical results by numerical examples with emphasis on the effect of the geometry on the bandgap and the transmission spectrum of the networks. Then we turn to the existence of localized modes within the gaps. The main conclusions are summarized in section 4.

2. Theoretical model

2.1. One-dimensional infinite serial loop structures

In this paper, we have calculated magnonic band structures and transmission coefficients for SLSs using the GFM developed by Dobrzynski [34]. The one-dimensional infinite serial loop

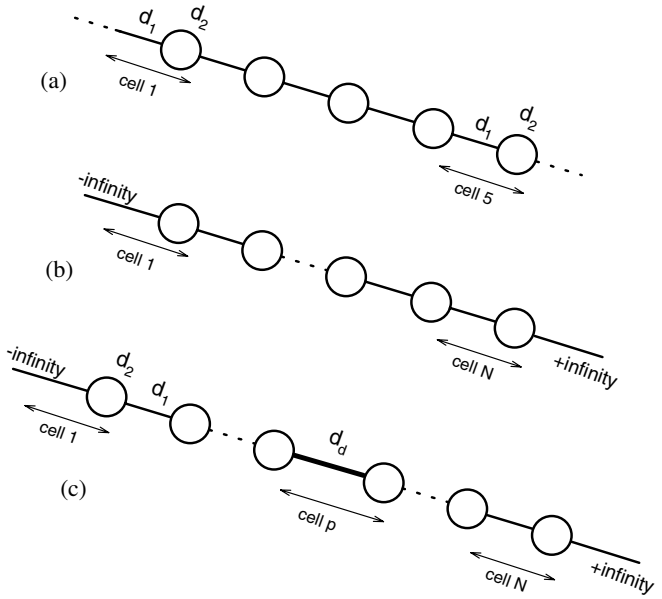

Figure 1. (a) Schematic diagram of the one-dimensional serial loop structure studied in this work. The media are designated by an index i, with i equal to 1 for the finite branch and 2 for the loop. Each loop has a length $2d_2$ and is distant by d_1 from neighbouring loops. Each cell is composed of a finite branch and the loop connected to its right extreme. (b) Waveguide with finite N loops separated by a length d_1 and connected at its extremities to two semi-infinite leading lines (medium 3). (c) The same as in (b) except that a defect branch of length d_d (heavy line) is introduced into cell p of the waveguide.

waveguide can be modelled as an infinite number of unit cells pasted together (see figure 1(a)). Each cell is composed of a finite wire (medium 1) of length d_1 in the direction x_3, connected to a loop 'ring' (medium 2) of length $2d_2$ (each loop is constructed of two wires with the same length d_2). The period of the SLS is $D = d_1 + d_2$. The interface domain is constituted of all the connection points between finite segments and loops. A space position along the x_3 axis in medium i belonging to the unit cell n is indicated by (n, i, x_3), where n, 'cell number', is an integer such that $-\infty < n < +\infty$, i the medium index and $-d_i/2 \leqslant x_3 \leqslant +d_i/2$. The media are assumed to be Heisenberg ferromagnets, which means that we are neglecting the dipole–dipole interaction as compared with the exchange contribution to the Hamiltonian [18]. Moreover, we are dealing with long-wavelength magnetic excitations and therefore use the continuum approximation of the Heisenberg model (see for details [15] and [18]). Here and afterwards the cross-sections of all wires are considered to be much smaller than the considered wavelength, so as to neglect the quantum size effect (or the sub-band structure). Due to the translational periodicity of the system in the direction x_3 one can define a wavevector k_3 along the axis of the waveguide associated with the period D. With these ingredients, one can derive analytically the dispersion relation of the SLS, as well as the transmission coefficient through a waveguide containing a finite number of loops.

The Green function of the infinite homogeneous ferromagnetic medium i associated with the magnetization satisfies the following equation [18]:

$$\frac{F_i}{\alpha_i}\left(\frac{\partial^2}{\partial {x_3}^2} - \alpha_i^2\right) G_i(x_3, x_3') = \delta(x_3 - x_3') \tag{1}$$

and can be expressed as

$$G_i(x_3, x_3') = -\frac{\mathrm{e}^{-\alpha_i|x_3 - x_3'|}}{2F_i} \tag{2}$$

where

$$F_i = \frac{D_i'\alpha_i}{\gamma_i M_i} \tag{3}$$

with

$$\alpha_i = \sqrt{-\frac{(\omega - \gamma_i H_0)}{D_i'}} \tag{4}$$

and

$$D_i' = \frac{2Ja^2 M_i}{\gamma_i \hbar^2}. \tag{5}$$

In equations (3)–(5), M_i, H_0, ω, J and γ_i represent, respectively, the spontaneous magnetization, the static external field in the x_1 direction, the frequency of the spin wave, the exchange interaction between neighbouring magnetic sites in the simple cubic lattice of lattice parameter a constituting the ferromagnetic medium and the gyromagnetic ratio.

We briefly recall the building principle of the Green function of the infinite SLS. This will enable us to present the dispersion relations and the transmitted waves without going into too much detail. Our calculation is based on the theory of interface response in composite materials [34], in which the Green function g of a composite system is given as

$$\begin{aligned} g(DD) = {} & G(DD) - G(DM)G^{-1}(MM)G(MD) \\ & + G(DM)G^{-1}(MM)g(MM)G^{-1}(MM)G(MD) \end{aligned} \tag{6}$$

where D and M are the whole space and the space of the interfaces in the composite materials, respectively. $G(DD)$ is the Green function of a reference continuous medium and $g(MM)$ the interface elements of the Green function of the composite system. The inverse $g^{-1}(MM)$ of $g(MM)$ is obtained for any point within the space of the interface $M = \{\bigcup M_i\}$ as a superposition of the different $g_i^{-1}(M_i, M_i)$ [34], the inverses of $g_i(M_i, M_i)$ for each constituent i of the composite system.

The interface states can be calculated from [34]

$$\det[g^{-1}(MM)] = 0 \tag{7}$$

showing that, if one is interested in calculating the interface states of a composite, one only needs to know the inverse of the Green function of each individual block in the space of their respective surfaces and/or interfaces.

Moreover if $U(D)$ [35] represents an eigenvector of the reference system, equation (6) enables the calculation of the eigenvectors $u(D)$ of the composite material

$$\begin{aligned} u(D) = {} & U(D) - U(M)G^{-1}(MM)G(MD) \\ & + U(M)G^{-1}(MM)g(MM)G^{-1}(MM)G(MD). \end{aligned} \tag{8}$$

In equation (8), $U(D)$, $U(M)$ and $u(D)$ are row-vectors. Equation (8) provides a description of all the waves reflected and transmitted by the interfaces, as well as the reflection and the transmission coefficients of the composite system. In this case, $U(D)$ must be replaced by a bulk wave launched in one homogeneous piece of the composite material [35].

Before addressing the problem of SLSs it is worthwhile as a first step to know the surface elements of the Green function of a finite wire of length d_i. The finite wire is bounded by two

free surfaces located at $x_3 = -d_i/2$ and $x_3 = +d_i/2$. These surface elements can be written [34] in the form of a (2×2) matrix $g_i(M_iM_i)$, within the interface space $M_i \equiv \{-d_i/2, +d_i/2\}$. The inverse of this matrix takes the following form:

$$[g_i(MM)]^{-1} = \begin{pmatrix} A_i & B_i \\ B_i & A_i \end{pmatrix} \tag{9}$$

where

$$A_i = -\frac{F_iC_i}{S_i} \tag{10a}$$

$$B_i = \frac{F_i}{S_i} \tag{10b}$$

with

$$C_i = \cosh(\alpha_i d_i), \tag{10c}$$

and

$$S_i = \sinh(\alpha_i d_i). \tag{10d}$$

Within the total interface space of the infinite SLS, the inverse of the matrix giving all the interface elements of the Green function g is an infinite tridiagonal matrix [34] formed by linear superposition of the elements $[g_i(MM)]^{-1}$. Taking into account the respective contributions of media 1 and 2 in the interface domain constituted of all the sites $(n, i, \pm d_1/2)$, this matrix takes the following form:

$$[g(MM)]^{-1} = \begin{pmatrix} B_1 & A_1+2A_2 & 2B_2 & \cdots & \cdots & \cdots \\ \cdots & 2B_2 & A_1+2A_2 & B_1 & \cdots & \cdots \\ \cdots & \cdots & B_1 & A_1+2A_2 & 2B_2 & \cdots \\ \cdots & \cdots & \cdots & 2B_2 & A_1+2A_2 & B_1 \end{pmatrix}. \tag{11}$$

Taking advantage of the translational periodicity of the system in the direction x_3, the above matrix can be Fourier transformed as

$$[g(\boldsymbol{k}, MM)]^{-1} = \begin{pmatrix} A_1+2A_2 & B_1+2B_2\mathrm{e}^{-\mathrm{j}kD} \\ B_1+2B_2\mathrm{e}^{\mathrm{j}kD} & A_1+2A_2 \end{pmatrix} \tag{12}$$

where k is the modulus of the one-dimensional reciprocal vector $\boldsymbol{k}$. In the $\boldsymbol{k}$ space, the Green function of the infinite SLS is obtained by inverting the above matrix, i.e.

$$[g(\boldsymbol{k}, MM)] = \frac{1/2}{\cos(kD) - \xi} \begin{pmatrix} Y_1 & \frac{S_2}{2F_2} + \frac{S_1}{F_1}\mathrm{e}^{-\mathrm{j}kD} \\ \frac{S_2}{2F_2} + \frac{S_1}{F_1}\mathrm{e}^{\mathrm{j}kD} & Y_1 \end{pmatrix} \tag{13}$$

where

$$\xi = C_1C_2 + \frac{1}{2}\left(\frac{F_1}{2F_2} + \frac{2F_2}{F_1}\right)S_1S_2 \tag{14}$$

and

$$Y_1 = \frac{C_2S_1}{F_1} + \frac{C_1S_2}{2F_2}. \tag{15}$$

The dispersion relation of the infinite serial loop waveguide is given by equation (7). This relation takes the simple form

$$\cos(kD) = \xi. \tag{16}$$

It is also straightforward to Fourier analyse back into real space all the elements of $g(\boldsymbol{k}, MM)$ and obtain all the interface elements of g, in the following form:

$$g(n, 1, +d_1/2; n', 1, +d_1/2) = g(n, 1, -d_1/2; n', 1, -d_1/2) = Y_1 \frac{t^{|n-n'|+1}}{t^2-1} \tag{17a}$$

$$g(n, 1, +d_1/2; n', 1, -d_1/2) = \frac{S_2}{2F_2}\frac{t^{|n-n'|+1}}{t^2-1} + \frac{S_1}{F_1}\frac{t^{|n-n'+1|+1}}{t^2-1} \tag{17b}$$

$$g(n, 1, -d_1/2; n', 1, +d_1/2) = \frac{S_2}{2F_2}\frac{t^{|n-n'|+1}}{t^2-1} + \frac{S_1}{F_1}\frac{t^{|n-n'-1|+1}}{t^2-1} \tag{17c}$$

where the integers n and n' refer to the cell number ($-\infty < n, n' < +\infty$) on the infinite waveguide and the parameter t is given by

$$t = \mathrm{e}^{\mathrm{j}kD}. \tag{18}$$

2.2. Transmission coefficient of the finite serial loop structures

Infinite magnonic SLSs are not physically realizable but finite loop structures are. Therefore, in this section, we investigate the transmission properties of a finite SLS. This structure is constructed as follows: a finite piece containing N equidistant loops is cut out of the infinite periodic system illustrated in figure 1(a), and this piece is subsequently connected at its extremities to two semi-infinite leading lines (medium 3). The finite SLS is therefore composed of N loops (medium 2; $2d_2$ is the length of each loop) pasted periodically with a finite segment (medium 1) of length d_1. We calculate analytically the transmission coefficient of a bulk spin wave from $x_3 = -\infty$.

The system of figure 1(b) is built from the infinite SLS illustrated in figure 1(a). *In a first step*, one suppresses the segment linking the loops lying in the cell 0 and in the cell 1 as well as the segment linking the loops lying in cell N and in cell $N + 1$. For this new system composed of a finite SLS and two semi-infinite leads, the inverse Green function at the interface space, $[g_t(MM)]^{-1}$, is an infinite banded matrix defined in the interface domain of all sites $(n, i, \pm d_1/2)$, $-\infty < n < +\infty$. This matrix is similar to that associated with the infinite SLS. Only a few matrix elements differ, namely those associated with the sites $(1, 1, -d_1/2)$, $(1, 1, +d_1/2)$, $(N + 1, 1, -d_1/2)$ and $(N + 1, 1, +d_1/2)$.

The cleavage operator $\boldsymbol{V}_{cl}(MM) = [g_t(MM)]^{-1} - [g(MM)]^{-1}$ [34] is the following 4×4 square matrix defined in the interface domain which is constituted of sites $(1, 1, -d_1/2)$, $(1, 1, +d_1/2)$, $(N + 1, 1, -d_1/2)$ and $(N + 1, 1, +d_1/2)$:

$$\boldsymbol{V}_{cl}(MM) = \begin{pmatrix} -A_1 & -B_1 & 0 & 0 \\ -B_1 & -A_1 & 0 & 0 \\ 0 & 0 & -A_1 & -B_1 \\ 0 & 0 & -B_1 & -A_1 \end{pmatrix}. \tag{19}$$

Using equations (17) and (19), one obtains the matrix operator $\triangle(MM) = \boldsymbol{I}(MM) + \boldsymbol{V}_{cl}(MM)\boldsymbol{g}(MM)$ in the space M of sites $(1, 1, -d_1/2)$, $(1, 1, +d_1/2)$, $(N + 1, 1, -d_1/2)$ and $(N + 1, 1, +d_1/2)$. For the calculation of the transmission coefficient, we need only the matrix elements $\triangle(1, 1, +d_1/2; 1, 1, +d_1/2)$, $\triangle(1, 1, +d_1/2; N + 1, 1, -d_1/2)$, $\triangle(N + 1, 1, -d_1/2; 1, 1, +d_1/2)$ and $\triangle(N + 1, 1, -d_1/2; N + 1, 1, -d_1/2)$, which can be set in the form of the 2×2 matrix $\triangle_s(MM)$

$$\triangle_s(MM) = \begin{pmatrix} 1 + \frac{-t(A_1Y_1+B_1Y_2')}{t^2-1} & \frac{-t^N(B_1Y_1t+A_1Y_2)}{t^2-1} \\ \frac{-t^N(B_1Y_1t+A_1Y_2)}{t^2-1} & 1 + \frac{-t(A_1Y_1+B_1Y_2')}{t^2-1} \end{pmatrix} \tag{20}$$

where

$$Y_2 = \frac{S_2}{2F_2}t + \frac{S_1}{F_1} \tag{21}$$

and

$$Y_2' = \frac{S_2}{2F_2} + \frac{S_1}{F_1}t. \tag{22}$$

The inverse surface Green function $[d_s(MM)]^{-1}$ of the finite SLS in the space of sites $(1, 1, +d_1/2)$ and $(N + 1, 1, -d_1/2)$ is given by

$$[d_s(MM)]^{-1} = \triangle_s(MM)[g_s(MM)]^{-1} \tag{23}$$

where

$$g_s(MM) = \frac{t}{t^2 - 1}\begin{pmatrix} Y_1 & t^{N-1}Y_2 \\ t^{N-1}Y_2 & Y_1 \end{pmatrix} \tag{24}$$

is the matrix constituted of elements of $g(MM)$ associated with sites $(1, 1, +d_1/2)$ and $(N + 1, 1, -d_1/2)$. From equation (23), simple algebra leads to

$$[d_s(MM)]^{-1} = \begin{pmatrix} A(N) & B(N) \\ B(N) & A(N) \end{pmatrix} \tag{25}$$

where

$$A(N) = \frac{Y_1Y_4 - t^{2N-2}Y_3Y_2}{Y_1^2 - t^{2N-2}Y_2^2} \tag{26}$$

$$B(N) = \frac{-Y_2Y_4 + Y_3Y_1}{Y_1^2 - t^{2N-2}Y_2^2}t^{N-1} \tag{27}$$

$$Y_3 = C_1 - C_2t \tag{28}$$

and

$$Y_4 = -\frac{1}{t} + C_1C_2 + \frac{F_1}{2F_2}S_1S_2. \tag{29}$$

In a second step, two semi-infinite leads (medium 3) are connected to the extremities $(1, 1, +d_1/2)$ and $(N + 1, 1, -d_1/2)$ of the finite SLS. With the help of the GFM [34], the inverse surface Green function $[d(MM)]^{-1}$ of the finite serial loops with two connected semi-infinite leads is given by

$$[d(MM)]^{-1} = \begin{pmatrix} A(N) - F_3 & B(N) \\ B(N) & A(N) - F_3 \end{pmatrix} \tag{30}$$

and consequently

$$\mathrm{d}(MM) = \frac{1}{(A(N) - F_3)^2 - B(N)^2}\begin{pmatrix} A(N) - F_3 & -B(N) \\ -B(N) & A(N) - F_3 \end{pmatrix} \tag{31}$$

where F_3 is the inverse surface Green function of the semi-infinite lead.

We now calculate the transmission coefficient with a bulk spin wave from $x_3 = -\infty$, $U(x_3) = \mathrm{e}^{-\alpha_3 x_3}$. Substituting this incident wave in equation (8) and considering equations (2) and (31), the transmission coefficient takes the form

$$T = \left|\frac{2F_3B(N)}{(A(N) - F_3)^2 - B(N)^2}\right|^2. \tag{32}$$

2.3. Transmission coefficient of a structure with a defect

The following section focuses on the existence of localized modes present within the gaps when a finite wire of length d_1 is replaced by a segment of length $d_d \neq d_1$ in one cell of the waveguide (see figure 1(c)). With the help of the GFM [34] one can arrive, analytically, at the following result for the localized states in the case of an infinite loop structure ($N \to \infty$):

$$\left\{1 + \frac{t}{t^2-1}(Y_1 - Y_2')(A_d - B_d + B_1 - A_1)\right\} \times \left\{1 + \frac{t}{t^2-1}(Y_1 + Y_2')(A_d + B_d - B_1 - A_1)\right\} = 0 \tag{33}$$

where A_d and B_d have the same definitions as A_i and B_i, which are given by equations (10*a*) and (10*b*).

Assuming that the defect is located in any cell of a finite SLS (see figure 1(c)), we have written an analytical expression for the transmission factor T through the defective waveguide

$$T = \left| \frac{2F_3 B(N) B(p) B_d}{Y_5 Y_5' - {B_d}^2 (A(N) - F_3)(A(p) - F_3)} \right|^2 \tag{34}$$

where

$$Y_5 = B^2(N) - (A(N) - F_3)(A(N) + A_d) \tag{35}$$

$$Y_5' = B^2(p) - (A(p) - F_3)(A(p) + A_d). \tag{36}$$

The integer p, such that $1 < p \leqslant N$, refers to the position of the defect cell in the waveguide and the rest of the symbols have their usual meaning.

3. Numerical results and discussion

We now illustrate these analytical results by a few numerical calculations for some specific examples. We report the results of dispersion relations and transmission factors with and without defects in the one-dimensional SLS. For the sake of simplicity, we have limited ourselves to the case where *identical media* ($F_1 = F_2 = F_3 = F_d$) constitute the SLS.

3.1. Magnonic bandgaps and transmission spectra

We start this section with a study of a simple example, namely a waveguide consisting of a unique loop. Equation (32) for the transmission factor T in the case of $N = 1$ can be written as

$$T = \frac{16}{25 - 9\cos^2(\alpha_2' d_2)} \tag{37}$$

where $\alpha_2' = -\mathrm{j}\alpha_2 = \sqrt{(\omega - \gamma_2 H_0)/D_2'}$.

This equation is identical to equation (9), which was given by Xia in [36]. The transmission coefficient *reaches its minimum value* of 16/25 when $\cos(\alpha_2' d_2) = 0$, i.e.

$$\alpha_2' d_2 = (m + \tfrac{1}{2})\pi. \tag{38}$$

The corresponding frequency is then

$$\omega_g = \gamma_2 H_0 + D_2' \left[(m + 1/2)\frac{\pi}{d_2}\right]^2 \tag{39}$$

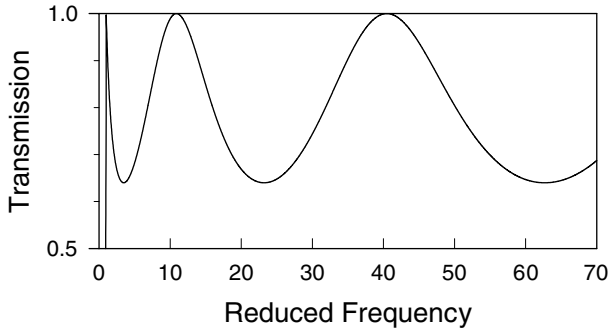

Figure 2. Transmission coefficient versus reduced frequency for a waveguide with one loop in the case of identical media 2 and 3. For convenience H_g is considered to be 1.

where m is a positive integer. Equation (39) can be rewritten in the dimensionless form

$$\Omega_g = H_g + [(m + 1/2)\pi]^2 \tag{40}$$

with $\Omega_g = \omega_g {d_2}^2/D_2'$ and $H_g = \gamma_2 H_0 {d_2}^2/D_2'$. It is noticeable from equation (37) that T reaches its maximum value of unity when $\alpha_2' d_2$ is a multiple of π. The variations of T versus the reduced frequency, $\Omega = \omega {d_2}^2/D_2'$, are reported in figure 2. In the case where $N > 1$, the minima of the transmission coefficient enlarge into gaps.

We now turn to the numerical results of the band structure and transmission coefficient for $N > 1$. In figure 3(a) the first five dispersion curves are shown in the band structure of the infinite serial loop composite with $d_1 = d_2$, and $N \longrightarrow \infty$. The plots are given as the reduced frequency $\Omega = \omega {d_1}^2/D_1' = \tilde{H} - \alpha_1^2 d_1^2$, with $\tilde{H} = \gamma_1 H_0 {d_1}^2/D_1'$, versus the dimensionless wavevector kD ($-\pi \leqslant kD \leqslant +\pi$). There is a complete absolute gap below the lowest band due to the presence of the external field H_0. There exist other absolute gaps, between the first and the second bands, the third and the fourth bands. The tangential points between the second and the third bands, on one hand, and the fourth and fifth bands, on the other hand, are degenerate points and they appear at $kD = 0$. Asymmetry is revealed between the second and the third bands as well as between the fourth and the fifth bands. This is reflected in the plot of the transmission factor. Figure 3(b) shows the frequency dependence of the transmission for $d_2 = d_1$ and $N = 10$. The number of oscillations in the transmission factor within the pass bands, which corresponds to the second and the third or to the fourth and fifth bands, has been noted to be unfailingly $2N - 1$. This number is $N - 1$ within the first pass band, which corresponds to the band that has no tangential points with any other bands (see also figure 3(d)).

Let us stress that, unlike the case in the usual one-dimensional (superlattice) or two-dimensional composite systems where the contrast in physical properties between the constituent materials is a critical parameter in determining the existence of the gaps [13–17], the occurrence of narrow magnonic bands *does not require the use of two different materials*. In other words, the magnonic structure is tailored within a single homogeneous medium although the boundary conditions impose the restriction that the waves propagate only in the interior of the waveguides.

In order to study the influence of the geometry of the SLS on its magnonic band structure, we have computed the band structure for $d_2/d_1 \neq 1$. For instance, figure 3(c) shows the first three bands for $d_2 = 0.3d_1$. It is noticeable that in this case the degenerate (tangential) points are removed and the bandgaps widen. A comparison between figures 3(a) and (c) reveals that the number of dispersion curves in the reduced frequency range, going from 0 to 60,

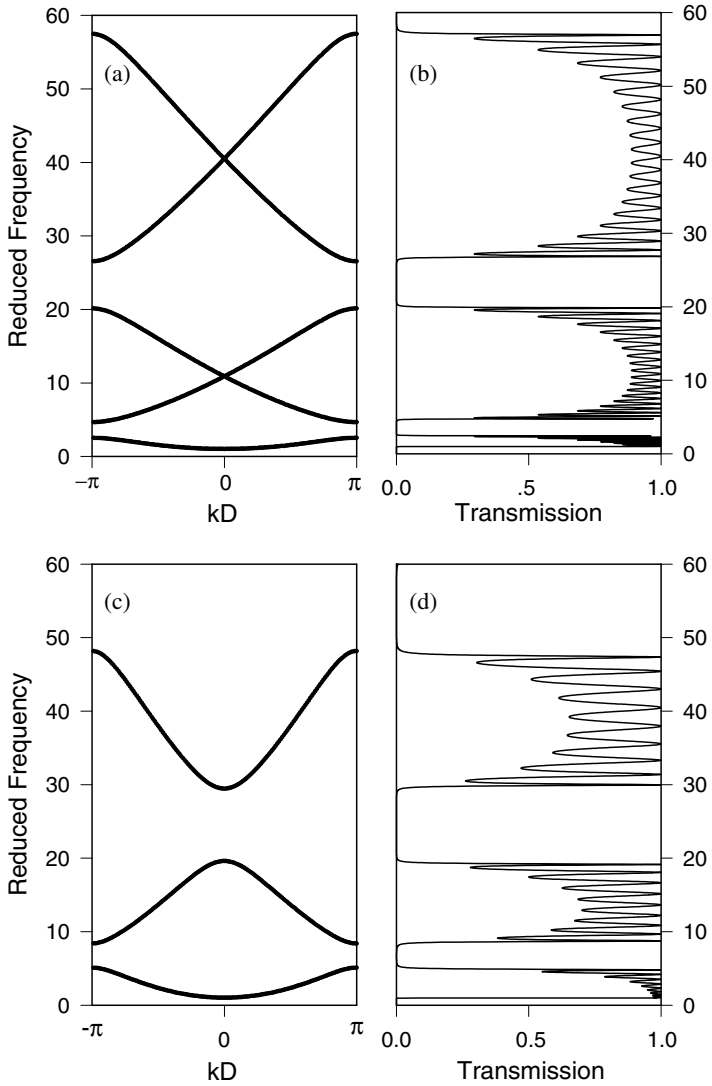

Figure 3. (a) The magnonic band structure of the infinite serial loop structure. We have chosen $d_1 = d_2$, $D_1' = D_2'$, $\tilde{H} = 1$ and $N \to \infty$. One observes an absolute gap below the first band due to the presence of the external field H_0. (b) Transmission spectrum versus the reduced frequency for a waveguide with $N = 10$. The other parameters are the same as in figure 3(a). (c) The same as in figure 3(a) but for $d_2 = 0.3d_1$. (d) The same as in figure 3(b) but for $d_2 = 0.3d_1$.

decreases when the ratio d_2/d_1 decreases. In other words, introducing such a deficiency in the geometry of the waveguide leads to a widening of the stop bands. The transmission factor is also influenced by this change of geometry. This phenomenon is illustrated in figure 3(d) for $N = 10$. Interestingly, the width of the pass bands (stop bands) decreases (increases) with this length d_2. Let us also underline the fact that the number of loops in the waveguide, N, is important in achieving completely formed gaps. This number is of the order of $N \approx 6$ where $d_2 = d_1$ (similar results are obtained for $d_2/d_1 = 0.5, 1, 1.5, 2, 2.5$), while it is of the order of $N \approx 8$ when $d_2 = 0.3d_1$.

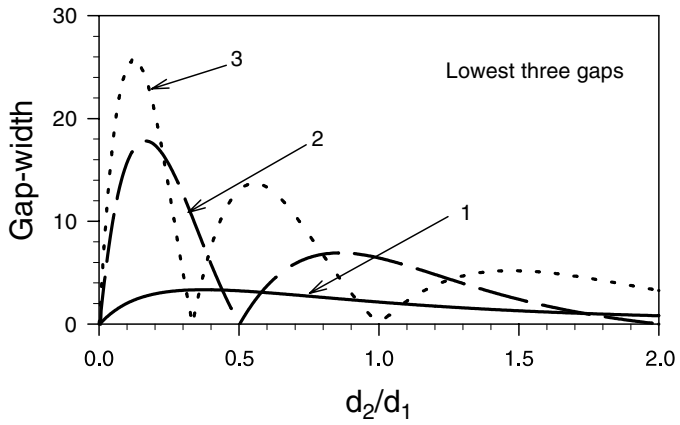

Figure 4. The variation of the gap-width of the first three magnonic bandgaps appearing in the band structure as a function of d_2/d_1. The numbers 1–3 refer to the first, second and third gaps, with increasing frequencies, in figure 3.

Figure 4 gives the evolution of the gap-width of the three lowest bandgaps in the one-dimensional SLS of figure 3. The gap-width on the y-axis represents the difference between the top and bottom frequencies of the absolute bandgaps as a function of d_2/d_1 in the range $0 < d_2/d_1 < 2$. As shown in figure 4, the second and the third gaps, respectively, close up for $d_2/d_1 = 0.5$ and 2, and $d_2/d_1 = 1/3$ and 1. All three gaps present a maximum width for $d_2/d_1 < 1$.

Figure 5 depicts the effect of the number N of loops on the transmission spectrum T for a finite SLS with $d_2/d_1 = 1$. We show the frequency dependence of the transmission for $N = 2, 6$ and 9 in the top, middle and bottom panels, respectively. One can see in the top panel for $N = 2$ that the transmission factor still does not reach the value zero i.e. there exists a partial transmission within the pseudo-gaps shown in this picture. It is apparent also that as N increases these pseudo-gaps in the transmission factor turn into full gaps. However, one does not need exceedingly large values of N. Indeed, at the relatively small value of $N = 6$ the gaps exist (note that the gap edge is however not yet sharp for $N = 6$). Moreover, for a given frequency range, there is an optimum value of the loop number above which any additional increase leaves the bands practically unaffected.

Finally, we end this section with a study of the influence of the number of loops on the geometry of the transmission factor when the ratio $d_2/d_1 \neq 1$. The results are displayed in figure 6, where $d_2/d_1 = 0.3$ is kept fixed, while N takes the values 2, 6 and 9 in the top, middle and bottom panels, respectively. Again we notice that the shrinking (widening) of the pass bands (stop bands) reveals the same behaviour as described in figure 5. For two different lengths d_1 and d_2, the oscillation amplitude decreases while the oscillation number is $N - 1$. Thus, the convergence to full gaps can be achieved in most cases for a reasonably small number of loops.

3.2. Defect modes and selective transmission

In this section, we discuss the existence of localized states present within the gaps when a defect is inserted in one cell of the waveguide (see figure 1(c)). Using equation (33), we studied the existence of localized modes as a function of the defect length. As mentioned before, we assume that our system is composed of identical media and $d_2/d_1 = 0.3$. Figure 7

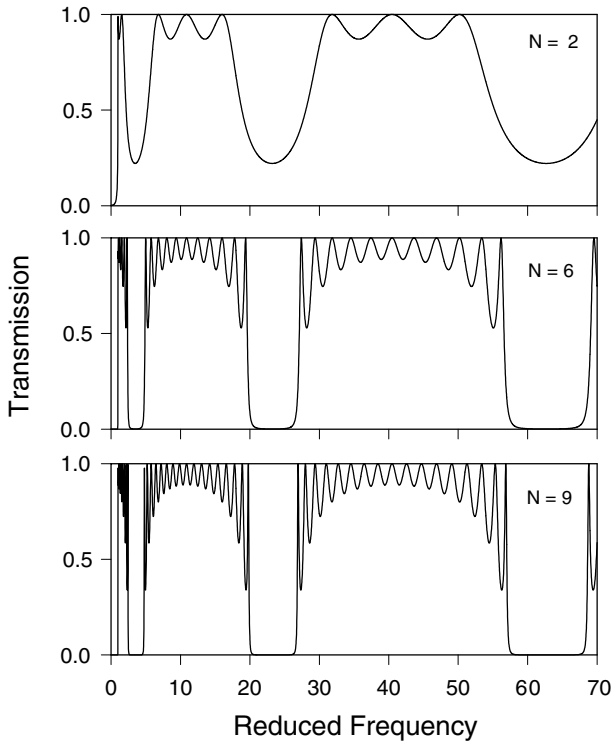

Figure 5. Evolution of the transmission spectrum versus the reduced frequency for several values of N. We have chosen $\tilde{H} = 1$, and $d_1 = d_2$. The top, middle and bottom panels depict the transmission for $N = 2$, 6 and 9, respectively. Note that increasing N results in turning some of the pseudo-gaps into complete gaps.

gives the frequencies of the localized modes as a function of the ratio d_d/d_1, where d_d is the length of the defect branch. The hatched areas correspond to the bulk bands of the perfect infinite SLS. The frequencies of the localized modes are very sensitive to the length d_d. The localized modes emerge from the bulk bands, decrease in frequency with increasing length d_d and finally merge into a lower bulk band, where they become resonant states. At the same time, new localized modes emerge from the bulk bands. One can notice that for any given reduced frequency in figure 7 there is a periodic repetition of the modes as functions of d_d/d_1.

The transmission spectrum is also affected by the presence of a defect branch inside the finite SLS. In particular, T (see equation (34)) exhibits narrow peaks associated with the localized modes. In figure 8, we compare the transmission coefficient for finite SLSs with and without defects. The results are illustrated for $N = 10$ and $d_2/d_1 = 0.3$. Figure 8(a) presents the transmission through a non-defective waveguide in the reduced frequency range going from 0 to 70 and is similar to that presented in figure 6(c). One observes in figure 8(b) that the presence of a defect branch of length $d_d = 1.3d_1$ in the middle of the waveguide (i.e. $p = 6$) gives rise to localized modes in the second, third and fourth gaps. The localized mode inside the third forbidden band lies in the middle of the gap while the localized modes in the other two gaps lie closer to the bulk bands. The second bulk band is asymmetric due to the proximity of the first localized mode to its left-hand side. The situation is similar for the third pass band, but the asymmetry is due to the proximity of the localized mode to its right. In the frequency range displayed in this figure, one can see that the peaks corresponding to

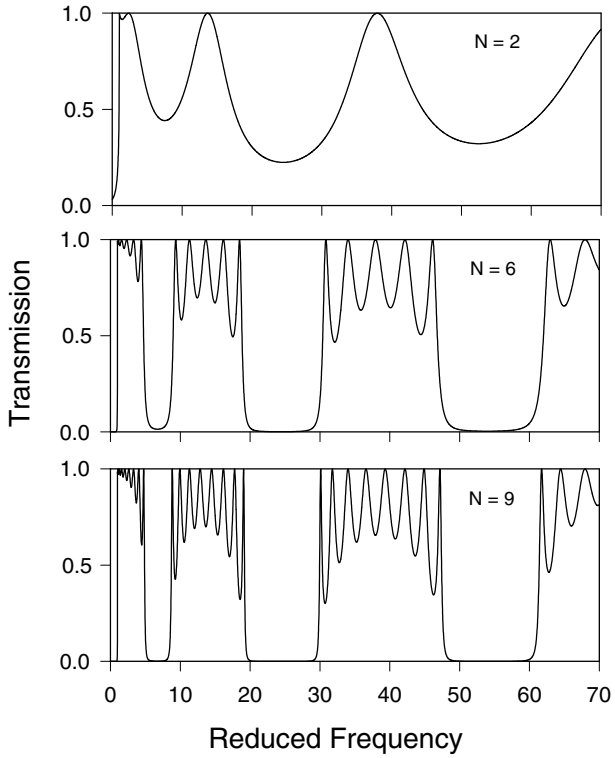

Figure 6. The same as in figure 5 but for $d_2 = 0.3d_1$. Attention is drawn to the increasing of the oscillation amplitudes with this choice of the length $d_2 \neq d_1$.

the localized modes are very narrow. The localized mode situated in the middle of the gap is more confined; i.e., the quality factor of the corresponding peak is greater. The transmission inside the pass bands is also affected nontrivially by the presence of a defect. The amplitude of the oscillations is much higher in the perturbed waveguide than in the perfect one. This behaviour is due to the presence of the defect branch in the middle of the waveguide. This forces the system to behave as two linked identical SLS waveguides with five loops. Each of these five-loop SLSs contributes in the same manner to the transmission depicted in figure 8(b). In particular, the transmission occurring inside the pass bands through each five loops presents the same number of oscillations with identical amplitude. This can have a constructive effect on the transmission of the defective waveguide, and this can explain why the oscillations are of stronger amplitude in figure 8(b) than those observed in figure 8(a). Finally, the last two panels of figure 8 demonstrate the influence of the position of the defect unit cell p on the transmission factor. In figures 8(c) and (d), the defect has been displaced from the centre of the structure (see figure 8(b)) to the seventh and eighth cells, respectively. In figure 8(c), there are six loops to the left of the defect and four to its right, while in figure 8(d) there are seven to the left of the defect and only three to its right. Unlike what is shown in figure 8(b), the ten-serial-loop structure behaves here as two linked waveguides with different numbers of loops. These two linked waveguides contribute in a different manner to the transmission of the defective structure, plotted in figures 8(c) and (d). In particular, the maxima and minima of transmission associated with each linked waveguide do not overlap. This may have a destructive effect on the transmission of the defective structure. In summary, the farther away the location of the

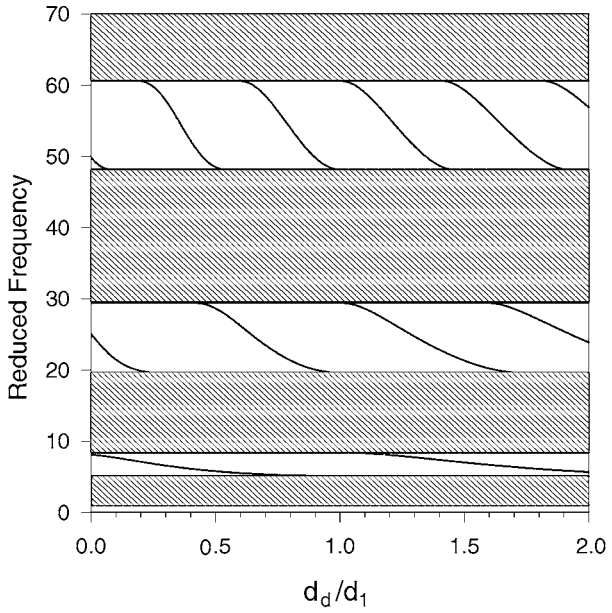

Figure 7. Frequencies of the localized modes associated with a defect branch of length d_{d}, inserted in an infinite serial loop structure. The other parameters are $N \longrightarrow \infty$, $d_2 = 0.3d_1$ and $\tilde{H} = 1$. The system is assumed to be composed of identical media.

defect branch from the middle of the waveguide, the stronger the depression in the transmission spectrum. In parallel, the closer the defect to the centre, the more confined the peak associated with the localized state.

Finally, we end this section with a study of the evolution of the intensity of the gap states as a function of the defect length d_{d}/d_1. The results are illustrated for three positions of the defect in figure 9(a). The plots are given for $N = 10$ and $d_2/d_1 = 0.3$. The hatched areas correspond to the pass bands of the structure. The dotted, dashed and full curves display the defect length dependence of the gap mode intensities for $p = 6, 7, 8$ respectively. We draw attention to the fact that the intensity of gap modes increases with the centralization of the defect inside the waveguide, and vice versa. One can also notice that for $p = 6$, i.e. the defect branch is placed in the middle of the structure, the intensity of the gap modes is equal to unity. This property is commonly verified when the composite system is symmetric, while it may only happen under special conditions if the composite system is asymmetric. For the sake of clarity, we have also sketched in figure 9(b) the frequencies of the localized modes as a function of the ratio d_{d}/d_1. (The hatched areas correspond to the bulk bands of the perfect infinite SLS.)

4. Summary and conclusions

In this paper we have presented a theoretical investigation of the magnonic band structure of one-dimensional SLS. Using a Green function method, we have obtained closed-form expressions for the band structure as well as for the transmission coefficients for an arbitrary value of the number N of loops in the structure. Absolute bandgaps exist in the spin wave band structure of an infinite SLS. The calculated transmission coefficient of magnons in finite

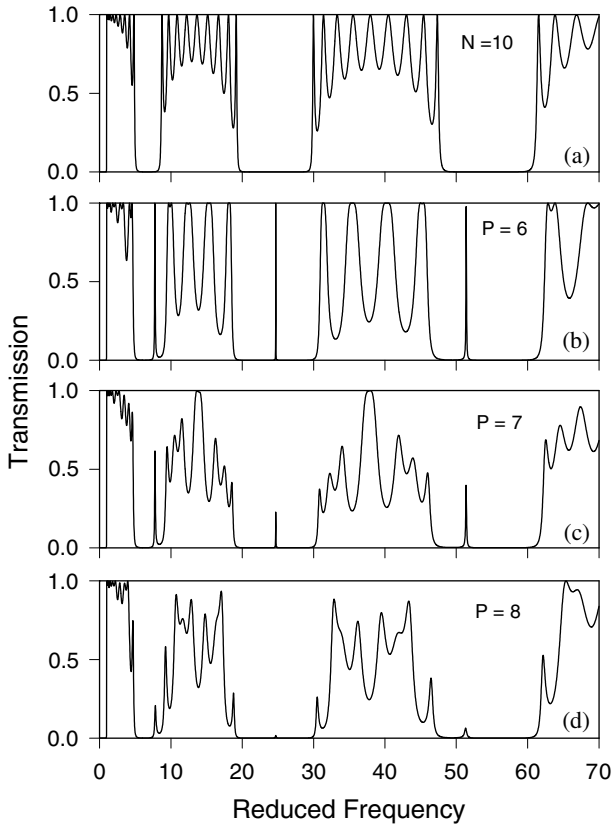

Figure 8. (a) Transmission spectrum versus the reduced frequency for a ten-loop SLS without defects. The other parameters are $\tilde{H} = 1$ and $d_2 = 0.3d_1$. (b) The same as in figure 8(a) but with one defect of length $d_d = 1.3d_1$ located in the middle of the waveguide, i.e. on the sixth cell. (c), (d) The same as in figure 8(b) but the defect is located on the seventh and eighth cells, respectively. In the frequency range displayed in (b), one can see that the peaks falling in the gaps are very narrow and present a strong amplitude. Transmission inside a bulk band is nontrivially affected by the presence of a defect. One notes the increase of the oscillation amplitudes. Panels (c) and (d) show that shifting the defect from the centre leads to a depression in the transmission factor inside the pass bands and reduces the amplitude of the peaks associated with the localized modes.

loop structures parallels the band spectrum of the infinite periodic SLS. The existence of the gaps in the spectrum is attributed to the periodicity of the geometry. In these systems, the gap width is controlled by the geometrical parameters as well as by the contrast in the physical properties of the constituents of the waveguide. Nevertheless, the magnonic band structure exhibits relatively wide gaps for homogeneous systems where the loops and the segments are constituted of the same material. We have also shown that waveguides composed of finite numbers of loops exhibit a behaviour similar to that of an infinite periodic SLS.

Analytical and numerical results on localized modes in perturbed waveguides were also reported. These localized modes result from the presence of a defect branch in the structure. These modes appear as narrow peaks of strong amplitude in the transmission spectrum when the defect is located in the middle of the waveguide. By changing the location of the defect in the waveguide, one affects significantly the transmission factor. Since it is generally the case that magnetic periodic networks have wide technical applications, it is anticipated that

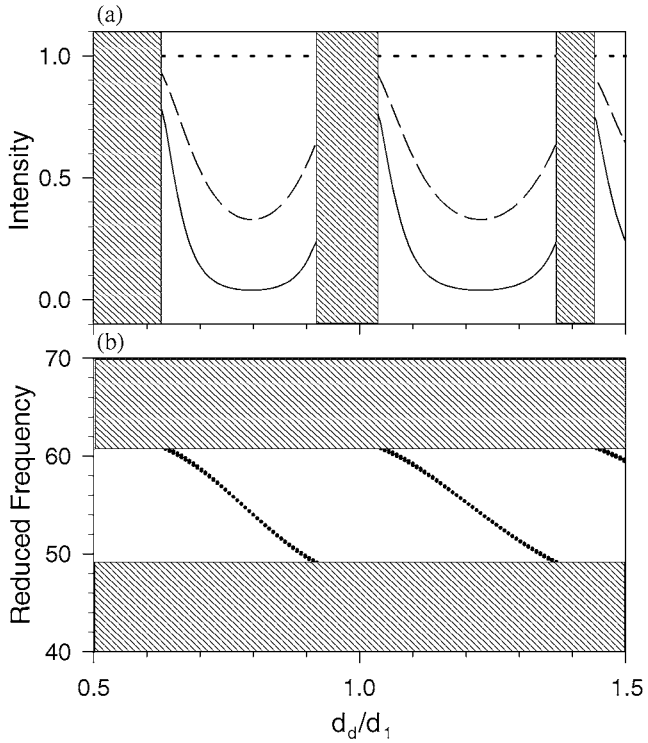

Figure 9. (a) Variation of the intensity of the transmitted gap modes as a function of the defect length d_d, inserted in a serial loop structure. The defect is situated on the sixth (dotted curves), seventh (dashed curves) and eighth (full curves) unit cell, respectively. The results are illustrated for $N = 10$, $d_2 = 0.3d_1$ and $\breve{H} = 1$. (b) Frequencies of the gap modes associated with a defect branch of length d_d.

this new class of materials, which can be referred to as 'magnonic crystals', will turn out to be of significant value for prospective applications. One would expect such applications to be feasible in spintronic devices, since magnon excitation energies also fall in the microwave range. Interestingly, the existence of a complete gap in these 'magnonic crystals' guarantees the perfect reflection (and hence an absence of transmission) of the excited spin wave within the frequency range of the stop band. The fabrication of such 'magnonic crystals' is of high interest because it will prohibit the transmission of spin waves within a desired forbidden frequency range. It is worth pointing out again that in all our calculations we have assumed that the cross section of the waveguide is small compared with the wavelength of the magnons.

It is relevant to direct attention here to some important differences between investigating the comblike structure (CLS) presented in [18] and the SLS presented in this paper. In the CLS we had to take into consideration the boundary conditions at the end of the resonators (dangling side branches); this problem is avoided in the present work for the SLS. In studying the transmission coefficient through a defective geometry, the defect branch in the CLS [18] was inserted (fixed) at the middle of the comb, while in the present work the defect can be located in any cell of the SLS, which in turn changes dramatically the transmission spectrum. It is also worth mentioning that when the defect wire is located in the middle of the SLS and whatever the ratio d_d/d_1 the intensities of the transmitted gap modes remain unity. However,

if the position of the defected cell is not in the middle, the intensity of the transmitted gap modes is remarkably depressed.

As a final remark, let us emphasize that our approach can only treat spin-wave excitations for isotropic Heisenberg ferromagnetic systems in which all the magnetizations are aligned to the same axis. The fact is that the spin wave is rather sensitive to the background spin configuration, which is again modified by the spin waves excited. Also the single-ion anisotropy, which is neglected in our approach, plays an important role in modelling real magnetic systems. A promising extension of the present work is to include explicitly the effects of the competition between exchange interaction and anisotropy, which generally results in complicated spin configuration and modifies the spin-wave spectrum.

Acknowledgment

A Mir and H Al Wahsh gratefully acknowledge the hospitality of the Laboratoire de Dynamique et Structure des Matériaux Moléculaires, Université de Lille 1.

References

[1] Greven M, Birgeneau R J and Wiese U J 1996 *Phys. Rev. Lett.* **77** 1865
[2] Chakravarty S 1996 *Phys. Rev. Lett.* **77** 4446
[3] Shelton D G, Nersesyan A A and Tsvelik A M 1996 *Phys. Rev.* B **53** 8521
Piekarewicz J and Shepard J R 1998 *Phys. Rev.* **57** 10 260
[4] Smyth J F, Schultz S, Fredkin D R, Kern D P, Rishton S A, Schmid H, Cali M and Koehler T R 1991 *J. Appl. Phys.* **69** 5262
[5] Maeda A, Kume M, Ogura T, Kukoori K, Yamada T, Nishikawa M and Harada Y 1994 *J. Appl. Phys.* **76** 6667
[6] Bardou N *et al* 1995 *J. Magn. Magn. Mater.* **148** 293
[7] Adeyeye A O, Bland J A C, Daboo C, Lee J, Ebels U and Ahmed H 1996 *J. Appl. Phys.* **79** 6120
[8] Mathieu C *et al* 1997 *Appl. Phys. Lett.* **70** 2912
[9] Ercole A, Adeyeye A O, Bland J A C and Haskooo D G 1998 *Phys. Rev.* B **58** 345
[10] Jorzick J, Demokritov S O, Mathieu C, Hillebrands B, Bartenlian B, Chappert C, Rousseaux F and Slavin A N 1999 *Phys. Rev.* B **60** 15 194
[11] DiVincenzo D P and Loss D 1998 *Superlatt. Microstruct.* **23** 419
Kane B E 1998 *Nature* **393** 133
[12] Mal'Shukov A G and Chao K A 2000 *Phys. Rev.* B **61** R2413
[13] Albuquerque E L, Falco P, Sarmento E F and Tilley D R 1986 *Solid State Commun.* **58** 41
[14] Krawczyk M, Lévy J-C, Mercier D and Puszkaski H 2001 *Phys. Lett.* A **282** 186
[15] Barnas J 1992 *Phys. Rev.* B **45** 10 427
[16] Hinchey L L and Mills D J 1986 *Phys. Rev.* B **33** 3359
Hinchey L L and Mills D J 1986 *Phys. Rev.* B **34** 1689
[17] Vasseur J O, Dobrzynski L, Djafari-Rouhani B and Puszkarski H 1996 *Phys. Rev.* B **54** 1043
[18] Al Wahsh H, Akjouj A, Djafari-Rouhani B, Vasseur J O, Dobrzynski L and Deymier P A 1999 *Phys. Rev.* B **59** 8709
[19] Yablonovitch E 1987 *Phys. Rev. Lett.* **58** 2059
[20] John S 1984 *Phys. Rev. Lett.* **53** 2169
[21] John S 1987 *Phys. Rev. Lett.* **58** 2486
[22] Kushwaha M S, Halevi P, Dobrzynski L and Djafari-Rouhani B 1993 *Phys. Rev. Lett.* **71** 2022
[23] Kushwaha M S and Halevi P 1996 *Appl. Phys. Lett.* **69** 31
Kushwaha M S and Djafari-Rouhani B 1996 *J. Appl. Phys.* **81** 3191
[24] Dobrzynski L, Djafari-Rouhani B, Vasseur J O, Kucharczyk R and Steslicka M 1995 *Prog. Surf. Sci.* **48** 213
[25] See for example, Joannopoulos J D, Meade R D and Winn J N 1995 *Photonic Crystals* (Princeton, NJ: Princeton University Press)
Joannopoulos J D, Meade R D and Winn J N 1996 *Photonic Band Gap Materials* ed C M Soukoulis (Dordrecht: Kluwer)
[26] Foresi S, Villeneuve P R, Ferrera J, Thoen E R, Steinmeyer G, Fan S, Joannopoulos J D, Kimerling L C, Smith H I and Ippen E P 1997 *Nature* **390** 143

[27] Vasseur J O, Deymier P A, Djafari-Rouhani B, Dobrzynski L and Akjouj A 1997 *Phys. Rev.* B **55** 10 434
Dobrzynski L, Akjouj A, Djafari-Rouhani B, Vasseur J O and Zemmouri J 1998 *Phys. Rev.* B **57** R9388
[28] See, e.g., Rai-Chaudhry P (ed) 1996 *The Handbook of Microlithography, Micromachining, and Microfabrication* (Bellingham, WA: SPIE Optical Engineering Press)
[29] Chou S Y, Wei M S, Krauss P R and Fisher P B 1994 *J. Appl. Phys.* **76** 6673
[30] Arias R and Mills D L 2001 *Phys. Rev.* B **63** 134439
[31] Encinas A, Demand M, Piraux L, Huynen I and Ebels U 2001 *Phys. Rev.* B **63** 104415
[32] Moul R C and Cottam M G 1979 *J. Phys. C: Solid State Phys.* **12** 5191
[33] Cottam M G 1979 *J. Phys. C: Solid State Phys.* **12** 1709
[34] Dobrzynski L 1990 *Surf. Sci. Rep.* **11** 139
[35] Dobrzynski L, Mendialdua J, Rodriguez A, Bolibo S and More M 1989 *J. Physique* **50** 2563
[36] Xia J B 1992 *Phys. Rev.* B **45** 3593